Development 138, 1005-1014 (2011) doi:10.1242/dev.051938

Cooperative activity of noggin and gremlin 1 in axial skeleton development

David A. Stafford[1,*], Lisa J. Brunet[1], Mustafa K. Khokha[1,†], Aris N. Economides[2] and Richard M. Harland[1,*]

SUMMARY

Inductive signals from adjacent tissues initiate differentiation within the somite. In this study, we used mouse embryos mutant for the BMP antagonists noggin (*Nog*) and gremlin 1 (*Grem1*) to characterize the effects of BMP signaling on the specification of the sclerotome. We confirmed reduction of *Pax1* and *Pax9* expression in *Nog* mutants, but found that *Nog*;*Grem1* double mutants completely fail to initiate sclerotome development. Furthermore, *Nog* mutants that also lack one allele of *Grem1* exhibit a dramatic reduction in axial skeleton relative to animals mutant for *Nog* alone. By contrast, *Pax3*, *Myf5* and *Lbx1* expression indicates that dermomyotome induction occurs in *Nog*;*Grem1* double mutants. Neither conditional *Bmpr1a* mutation nor treatment with the BMP type I receptor inhibitor dorsomorphin expands sclerotome marker expression, suggesting that BMP antagonists do not have an instructive function in sclerotome specification. Instead, we hypothesize that Nog- and Grem1-mediated inhibition of BMP is permissive for hedgehog (Hh) signal-mediated sclerotome specification. In support of this model, we found that culturing *Nog*;*Grem1* double-mutant embryos with dorsomorphin restores sclerotome, whereas *Pax1* expression in smoothened (*Smo*) mutants is not rescued, suggesting that inhibition of BMP is insufficient to induce sclerotome in the absence of Hh signaling. Confirming the dominant inhibitory effect of BMP signaling, *Pax1* expression cannot be rescued in *Nog*;*Grem1* double mutants by forced activation of Smo. We conclude that *Nog* and *Grem1* cooperate to maintain a BMP signaling-free zone that is a crucial prerequisite for Hh-mediated sclerotome induction.

KEY WORDS: Sclerotome, BMP antagonist, Hedgehog signaling, Mouse

INTRODUCTION

Somites are bilateral metameric structures that form from the mesoderm that flanks the neural tube and notochord. Starting as uncommitted epithelial spheres, somites rapidly differentiate into the dorsal-lateral dermomyotome, which contains the precursors for skeletal muscles and dermis, and ventral-medial sclerotome, which gives rise to the bone and cartilage of the axial skeleton. Embryological and genetic analyses have identified the inductive interactions and molecular signals that initiate somite pattern formation. Sclerotome is specified by sonic hedgehog (Shh) derived from the notochord and floor plate. These tissues, or Shh alone, induce sclerotome marker expression in cultured paraxial mesoderm (Borycki et al., 1998; Fan and Tessier-Lavigne, 1994; Marcelle et al., 1999; Murtaugh et al., 1999; Teillet et al., 1998). Furthermore, *Shh* mutant embryos fail to form an axial skeleton (Chiang et al., 1996) and sclerotome markers are not expressed in embryos mutant for the obligate hedgehog (Hh) signal-activating receptor smoothened (*Smo*) (Zhang et al., 2001). Embryos lacking both Gli2 and Gli3, which along with Gli1 are the major transcription factors that mediate Hh signaling, also fail to form sclerotome (Buttitta et al., 2003). Shh induces expression of the sclerotome-specific transcription factors Pax1 and Pax9, which have redundant roles in the formation of the vertebral column (Peters et al., 1999).

[1]Department of Molecular and Cell Biology and Center for Integrative Genomics, University of California, Berkeley, California 94720, USA. [2]Regeneron Pharmaceuticals, Tarrytown, NY 10591-6707, USA.

*Authors for correspondence (dastaffo@berkeley.edu; harland@berkeley.edu)
†Present address: Department of Pediatrics and Genetics, Yale University School of Medicine, New Haven, CT 06520, USA

Accepted 17 December 2010

The effect of Hh signaling on sclerotome development depends stage specifically on BMP signaling. Chick presomitic mesoderm (PSM) explants initiate cartilage marker expression in response to BMP through a Sox9 and Nkx3.2 autoregulatory loop (Zeng et al., 2002), provided that the tissue has first been exposed to Shh (Murtaugh et al., 1999). In addition, BMP-secreting cells induce the formation of superficial dorsal cartilage (Monsoro-Burq et al., 1996). By contrast, early BMP exposure interferes with vertebral development. Treatment of chick PSM with BMP4 blocks all sclerotome and chondrocyte marker expression (Murtaugh et al., 1999), whereas ventrally positioned BMP4-expressing cells prevent formation of lateral aspects of the vertebra (Monsoro-Burq et al., 1996). Mice lacking the secreted BMP antagonist noggin (*Nog*) provide genetic evidence for the variable effect of BMP on the development of the axial skeleton; *Nog* mutant embryos exhibit delayed sclerotome marker expression and loss of caudal vertebrae but an excess of cartilage formation in anterior ribs and vertebrae (Brunet et al., 1998; McMahon et al., 1998).

Although the *Nog* phenotype demonstrates the importance of BMP antagonist function in axial skeletal development, our understanding is incomplete. Caudal vertebral development in *Nog* mutants is partially restored by a reduction in BMP signaling (Wijgerde et al., 2005), showing that caudal sclerotome development depends on the local integration of BMPs and Nog. High expression of Bmp4 in the posterior lateral plate might dictate a need for Nog in the nearby somites, but there might be no requirement for such regulation in the anterior domain. Additionally, the mechanism by which Nog promotes sclerotome specification is not defined. Based on the capacity of Nog to induce *Pax1* expression in the presence of reagents that inhibit Hh signal transduction, it has been suggested that Nog might induce sclerotome independently of Hh (McMahon et al., 1998).

Furthermore, although it is clear that BMP can inhibit sclerotome specification, the mechanism underlying this suppression is unknown.

Multiple BMP antagonists are expressed during mouse gestation, and compensation by other antagonists might explain the variable consequences of *Nog* mutation for axial skeleton development. *Nog*;*Chrd* double mutants exhibit deficiencies in the derivatives of anterior mesoderm, including cervical vertebrae (Bachiller et al., 2000). However, this was attributed to a lack of rostral *Shh* and is therefore distinct from the defect exhibited by *Nog* mutants, which have a notochord and express Shh (McMahon et al., 1998). Thus, the question of whether multiple antagonists contribute to sclerotome development remains open.

The DAN family member antagonist gremlin 1 (*Grem1*) is expressed in PSM and newly formed somites starting at E8.5 (Pearce et al., 1999) and is a candidate factor for regulating axial skeletal development. Although *Grem1* mutants have no apparent somite phenotype (Khokha et al., 2003), we hypothesized that ablating *Grem1* in combination with *Nog* might result in more severe consequences for somite pattern formation. We show that removing both *Nog* and *Grem1* causes the loss of the sclerotome. We also demonstrate that the elevated BMP signaling in these mutants affects the outcome of the Hh signals that underlie sclerotome specification.

MATERIALS AND METHODS

Generation of mice

A conditional *Nog* targeting construct was made using genomic DNA clones previously used to make the *Nog* null mutant (McMahon et al., 1998). Briefly, a pgk-Neo cassette flanked by FRT sites and followed by a single lox site was inserted into the unique *Eco*RI site 1959 bp downstream of the ATG initiation codon. An *Xba*I site followed by a lox site was inserted into the unique *Not*I site located 252 bp upstream of the ATG initiation codon. A pgk-diphtheria toxin cassette was located upstream of the 5′ arm of homology. This construct was electroporated into E14 mouse embryonic stem (ES) cells and colonies were selected for resistance to G418. Positive colonies were subjected to Southern analysis with 5′ and 3′ probes. One positive clone out of 2400 was injected into blastocysts. Heterozygous pups containing the conditional transgene were mated to B6;SJL-Tg(ACTFLPe)9205Dym/J mice to delete the pgk-Neo cassette. Mice were then bred to FVB/N-Tg(ACTB-Cre)2Mrt/J. Primers used to distinguish conditional *Nog* were 5′-ACAGAGAAACAAGACGCC-3′ and 5′ACGAGTTGGTCGCAATTCC-3′. The wild-type product is ~200 bp and the conditional product is ~250 bp. Upon deletion of the region flanked by lox sites, a 400 bp product is generated using 5′-AGGCTCCGCACAGAGAAACAAG-3′ and 5′-GAGTAAATGTCCA-GGGAAGGGG-3′.

The *Nog* mutant phenotype depends on the strain background (McMahon et al., 1998; Tylzanowski et al., 2006). Unless noted otherwise, experiments reported here used mice from a mixed C57/B6;129/Ola;FVB background, in which the *Nog* phenotype is relatively mild, closely resembling the phenotype reported for FVB or Dba1 backgrounds (Tylzanowski et al., 2006). More severe phenotypes cause neural tube and other morphological defects that obscure interpretation of the effects of *Grem1* mutation.

In situ hybridization and immunofluorescence

mRNA was stained by in situ hybridization (Nagy et al., 2003) and apoptotic cells revealed by TUNEL (Boehringer Mannheim, 12 156 792 910) according to the manufacturer's instructions. For immunofluorescence, embryos were dissected and fixed in 4% paraformaldehyde/1×PBS for 30 minutes. Following overnight incubation in 30% sucrose/1×PBS, trunk sections were embedded in Neg-50 (Thermo-Fisher) and sectioned at 12 μm using a Microm 550 OMVP cryostat. Sections were blocked with 10% goat serum/1×PBS/0.3% Triton X-100 and incubated with primary antibodies at the following dilutions: phosphorylated histone H3 (Millipore/Upstate, 06-570) at 1:500; and protein kinase C (Santa Cruz, 101777) at 1:200. Alexa Fluor 488- or 555-conjugated secondary antibodies (Molecular Probes/Invitrogen) were used at 1:500. Other stains include: phalloidin 488 (Molecular Probes/Invitrogen, A12379) at 0.5 U/ml; Hoechst (Molecular Probes/Invitrogen, H3570) at 1:2000; and Draq5 (BioStatus, DR50050) at 1:5000.

Cultures

Whole E8.5 mouse embryos were cultured as described (Nagy et al., 2003) with the following modifications. Medium contained a 2:1 mixture of rat serum (Harlan):DMEM, with penicillin/streptomycin and drug/vehicle control. Dorsomorphin (Sigma) was diluted from 10 mM in DMSO to a working concentration of 5 μM. Purmorphamine (Cayman) was diluted from 25 mM in DMF to 7.5 μM. Embryos were cultured individually in 1 ml medium in sterile 14-ml polypropylene tubes in a standard tissue culture incubator at ambient atmosphere with 5% CO_2 for 30 hours. Rotation (14 rpm) at an angle of 45° was maintained. This protocol reliably supported growth of post-implantation embryos up to Theiler stage 16, with only rare occurrences of turning or neural tube closure defects in controls. Somite micromass cultures were performed as described (Winnier et al., 1997).

Quantitative PCR

cDNA was synthesized from Trizol-extracted total RNA using standard methods. Expression was assessed by quantitative (Q) PCR with SYBR Green reagents on an Applied Biosystems 7300 system using β-actin as an internal reference. Primer sequences are provided in Table S1 in the supplementary material.

RESULTS

Expression of *Nog* and *Grem1* during somite patterning

In the developing mouse somite, the expression of markers of sclerotome and dermomyotome initiates from early embryonic day (E) 8.5 to E9.0. At these stages, *Nog* and *Grem1* are expressed in the midline and somites, respectively, consistent with roles in somite patterning (McMahon et al., 1998; Pearce et al., 1999). We revisited the expression of *Nog* and *Grem1* between E8.5 and E9.0 with an emphasis on the developing trunk (Fig. 1). E8.5 embryos expressed *Nog* throughout the notochord and dorsal neural tube (Fig. 1A,A′). Immediately following turning, *Nog* expression was diminished in the anterior notochord but remained in the posterior notochord and the roof plate (Fig. 1B). This pattern persisted to E9.5, at which point *Nog* expression initiated in the medial lip of the dermomyotome (Fig. 1C). *Grem1* was expressed at E8.5 in recently formed somites as well as in presomitic and lateral plate mesoderm and posterior dorsal neural tube (Fig. 1D,D′). As the embryo initiated turning *Grem1* expression became restricted to the lateral dermomyotome (Fig. 1E). Similar to *Nog*, *Grem1* expression could also be detected in the E9.5 medial dermomyotome (Fig. 1F). This analysis confirms that, although not expressed in overlapping domains, *Nog* and *Grem1* could potentially have overlapping functions in early somite patterning.

Generation of *Nog* and *Grem1* mouse mutants

Although capable of forming somites and initiating early somite patterning, *Nog* mutants exhibit clear deficiencies in the development of somite-derived tissues (McMahon et al., 1998). Based on their concurrent expression and similar molecular properties (Hsu et al., 1998; Zimmerman et al., 1996), we hypothesized that mutations in *Grem1* might enhance the *Nog* mutant phenotype. To increase the recovery of mutants, we used conditional mutants to test the additive effect of *Grem1* ablation on the somite phenotype in *Nog* mutants. Using homologous recombination in ES cells, we introduced loxP

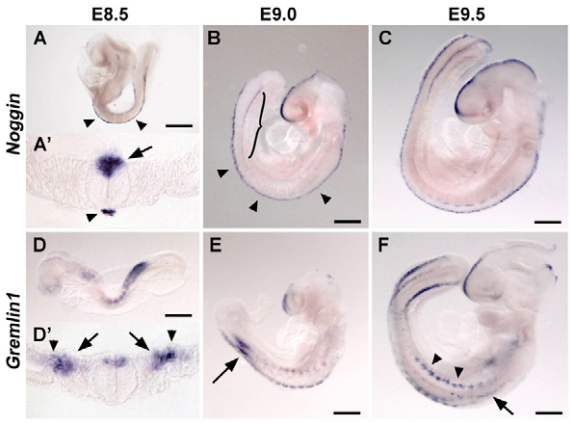

Fig. 1. *Nog* and *Grem1* expression during somite pattern formation. Whole-mount in situ hybridization for mouse *Nog* (A,A′,B,C) and *Grem1* (D,D′,E,F). (**A**) E8.5 *Nog* expression in the notochord (arrowheads) and dorsal neural tube. (**A′**) Transverse section through somite 6 showing E8.5 *Nog* expression in the dorsal neural tube (arrow) and notochord (arrowhead). (**B**) *Nog* is expressed at E9.0 in the dorsal neural tube (arrowheads) but has become restricted to the posterior notochord (bracket). (**C**) At E9.5, *Nog* expression is detectable in the tail notochord, dorsal neural tube and medial dermomyotome. (**D**) E8.5 *Grem1* expression in the recently formed somites and posterior paraxial mesoderm. (**D′**) Transverse section through somite 6 showing E8.5 *Grem1* expression in the dorsal neural tube, dorsal-lateral somite (arrows) and lateral plate mesoderm (arrowheads). (**E**) At E9.0, somitic *Grem1* expression is restricted to the lateral dermomyotome. Expression also appears in the posterior dorsal neural tube and lateral mesoderm (arrow). (**F**) E9.5 *Grem1* expression is concentrated in the lateral dermomyotome (arrowheads) and has initiated in the medial dermomyotome of anterior somites (arrow). Lateral views, facing left. Scale bars: 300 μm.

Cre recognition sites flanking the single-exon *Nog* gene. This was used to generate a conditional *Nog* mutant line ($Nog^{fx/fx}$). We used a previously generated conditional *Grem1* mutant line ($Grem1^{fx/fx}$) (Gazzerro et al., 2007). Female homozygotes ($Nog^{fx/fx}$ or $Grem1^{fx/fx}$) were crossed to heterozygous males ($Nog^{fx/+}$ or $Grem1^{fx/+}$) that were also homozygous for constitutively active β-*actin-Cre* (Lewandoski et al., 1997). Thus, all offspring receive a single β-*actin-Cre* transgene and half the embryos are homozygous for the conditional allele. The homozygous conditional *Nog* and *Grem1* mutants phenocopied conventional nulls (see Fig. S1 in the supplementary material). At E16.5, *Nog* homozygous conditional mutants exhibited the characteristic broad autopods, neural tube defects and stunted tails (McMahon et al., 1998). *Grem1* homozygous conditional mutants had the characteristic deformed limbs (Khokha et al., 2003). QPCR confirmed efficient loss of each allele. In $Grem1^{fx/fx}$ embryos, *Grem1* expression was 0.015% that of $Grem1^{fx/+}$ littermates. *Nog* expression in $Nog^{fx/fx}$ embryos was less than 0.010% of $Nog^{fx/+}$ levels.

To generate embryos lacking both *Nog* and *Grem1*, female double homozygotes ($Nog^{fx/fx}$;$Grem1^{fx/fx}$) were crossed to double-heterozygous males ($Nog^{fx/+}$;$Grem1^{fx/+}$) that were homozygous for β-*actin-Cre*. This strategy increases the number of double mutants 4-fold over a strategy involving intercrossed double-heterozygous null mutants, producing equal numbers of the following four genotypes: $Nog^{fx/+}$;$Grem1^{fx/+}$, used as controls; $Nog^{fx/fx}$;$Grem1^{fx/+}$, also referred to as *Nog* mutants; $Nog^{fx/+}$;$Grem1^{fx/fx}$, also referred to as *Grem1* mutants; and $Nog^{fx/fx}$;$Grem1^{fx/fx}$, also referred to as double mutants.

Nog and *Nog;Grem1* mutant embryos have impaired somite formation

For dissections prior to E9.5, we collected embryos of the four possible genotypes at approximately the expected 1:1:1:1 ratio (see Fig. S1 in the supplementary material). We recovered fewer double mutants from later dissections; at E9.5, we obtained 65% of the predicted frequency of double mutants, whereas the other classes were represented as expected (see Fig. S1D in the supplementary material). $Nog^{fx/+}$;$Grem1^{fx/+}$ embryos appeared normal at all stages examined and throughout adulthood (Fig. 2A). There are no reported defects in embryos lacking *Grem1* prior to E10.5. Likewise, $Nog^{fx/+}$;$Grem1^{fx/fx}$ embryos appeared as wild type at E8.5-9.5 (Fig. 2B). On this background, the phenotype of $Nog^{fx/fx}$;$Grem1^{fx/+}$ E8.5-9.5 embryos resembled that of homozygous *Nog* null mutants (McMahon et al., 1998), exhibiting small posterior somites and buckled neural tubes that frequently failed to close anteriorly (Fig. 2C). The morphological defects of double-mutant embryos ($Nog^{fx/fx}$;$Grem1^{fx/fx}$) were invariably more severe than those observed in $Nog^{fx/fx}$;$Grem1^{fx/+}$ siblings (Fig. 2D). The neural tube was highly kinked and both the neural tube and brain failed to fuse dorsally. In contrast to $Nog^{fx/fx}$;$Grem1^{fx/+}$ embryos, central nervous system development anterior to the midbrain arrested in the double mutants. Owing to arrested growth caudal to the thoracic trunk, double-mutant embryos were shorter than the other genetic classes.

To characterize the consequences of *Nog*;*Grem1* mutation for somite formation, we assessed the expression of *Meox1*, which encodes a transcription factor that is initially expressed throughout the epithelial somite (Candia et al., 1992) and, along with *Meox2*, is required for the chondrogenesis and myogenesis of paraxial mesoderm (Mankoo et al., 2003). At E9.5, double-heterozygous control and *Grem1* mutant ($Nog^{fx/+}$;$Grem1^{fx/fx}$) embryos expressed *Meox1* throughout the somites (Fig. 2E,F). In *Nog* mutants, somitic *Meox1* expression at E9.5 highlighted the characteristic progressive reduction in somite size in the lumbar region, although expression was present in the hindlimb region (Fig. 2G). In double mutants, the caudal expression domain was also lost (Fig. 2H). Consistent with a requirement for *Grem1* in this region, *Grem1* was expressed normally in the PSM and was still present in *Nog* mutant embryos (not shown).

Some of the differences in somite size were already apparent at E9.0, although the severity of reduction in the *Nog* homozygotes at somites 8-12 was not increased by ablation of *Grem1* (Fig. 2J,K). Transverse sections showed disordered *Meox1* staining extending over a smaller area in both $Nog^{fx/fx}$;$Grem1^{fx/+}$ and $Nog^{fx/fx}$;$Grem1^{fx/fx}$ embryos relative to controls. To better characterize somite morphology, we stained somites for filamentous actin (F-actin), which marks the internal surface of the epithelial somite. The somitocoele was clearly demarcated in control sections (Fig. 2L). *Nog* and double-mutant somites showed disorganized F-actin accumulation within the somite, suggesting that epithelium formation is compromised in the thoracic somites of these embryos (Fig. 2M,N). Equivalent results were obtained with samples stained with an antibody to atypical protein kinase C (Fig. 2L-N). We conclude that *Nog* is required for the formation of the first 15-20 somites and that *Grem1* mutation does not exacerbate this somitogenesis phenotype. By contrast, in the absence of *Nog*, *Grem1* is sufficient to allow axis elongation and paraxial mesoderm development in posterior aspects of the embryo.

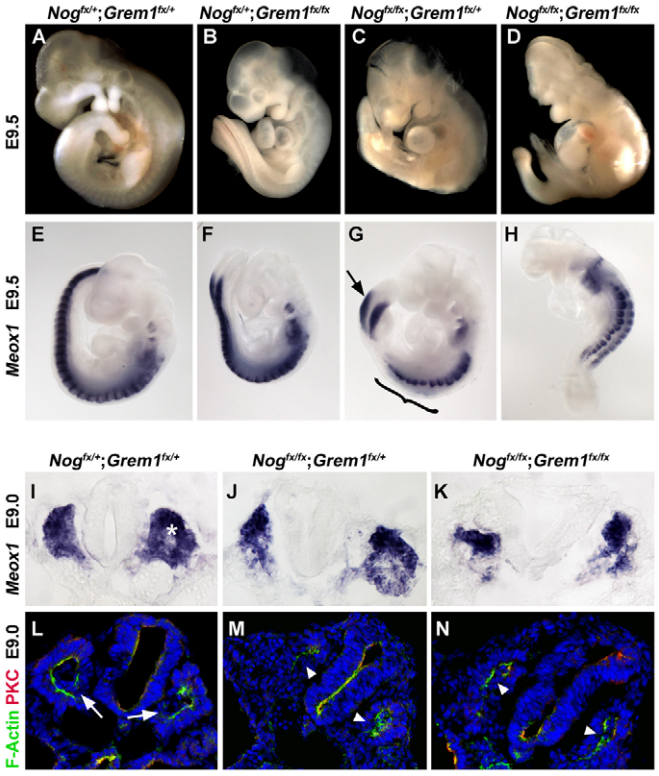

Fig. 2. *Nog* mutants and *Nog;Grem1* mutant mouse embryos have impaired somite formation. (**A**) E9.5 *Nog*$^{fx/+}$;*Grem1*$^{fx/+}$ embryo. This genetic class resembles the wild-type condition. (**B**) A *Nog*$^{fx/+}$;*Grem1*$^{fx/fx}$ embryo. There are no evident developmental consequences of *Grem1* mutation at E9.5. (**C**) A *Nog*$^{fx/fx}$;*Grem1*$^{fx/+}$ embryo. At E9.5, *Nog* mutants exhibit small posterior somites and kinked neural tubes. (**D**) A *Nog*$^{fx/fx}$;*Grem1*$^{fx/fx}$ embryo. Double-mutant embryos have severe defects in neural tube, somite, head and tail development. (**E-H**) Whole-mount E9.5 in situ hybridizations for the somite marker *Meox1*; lateral views, facing left. A minimum of five embryos were examined for each genetic class. (E,F) *Nog*$^{fx/+}$;*Grem1*$^{fx/+}$ (E) and *Nog*$^{fx/+}$;*Grem1*$^{fx/fx}$ (F) embryos appear as wild type. (G) A *Nog*$^{fx/fx}$;*Grem1*$^{fx/+}$ embryo showing reduced somite size from somites 7-15 (bracket), an absence of *Meox1* expression in the lumbar region, and a restoration of signal in the tailbud (arrow). (H) A *Nog*$^{fx/fx}$;*Grem1*$^{fx/fx}$ double-mutant embryo. Whereas *Meox1* expression is similar to that in *Nog* mutants in anterior somites, no expression appears posterior to somite 15. (**I-K**) E9.0 in situ hybridizations for *Meox1*. Transverse sections through the trunk between somites 8-12. (I) Somites of *Nog*$^{fx/+}$;*Grem1*$^{fx/+}$ embryos have clear epithelial morphology and somitocoele (asterisk). (J,K) *Nog*$^{fx/fx}$;*Grem1*$^{fx/+}$ (J) and *Nog*$^{fx/fx}$;*Grem1*$^{fx/fx}$ (K) somites are disorganized and reduced in size. (**L-N**) Transverse sections through the trunk between somites 8-12 of E9.0 embryos stained for F-actin (green) and atypical protein kinase C (PKC, red) to mark the apical (internal) surface of the epithelial somite. Three embryos of each genotype were examined. (L) Somites of *Nog*$^{fx/+}$;*Grem1*$^{fx/+}$ embryos show F-actin and PKC accumulation at the apical surface. The discontinuity in the stain medially (arrows) indicates the epithelial-to-mesenchymal transition associated with sclerotome formation. (M,N) Epithelium formation in *Nog*$^{fx/fx}$;*Grem1*$^{fx/+}$ (M) and *Nog*$^{fx/fx}$;*Grem1*$^{fx/fx}$ (N) somites (arrowheads) is aberrant.

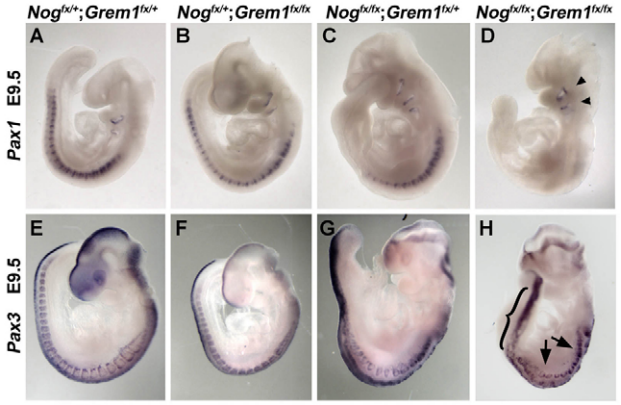

Fig. 3. *Nog;Grem1* double-mutant mouse embryos lack sclerotome. (**A-D**) Whole-mount E9.5 in situ hybridizations for the sclerotome marker *Pax1*; lateral views. (A,B) *Nog*$^{fx/+}$;*Grem1*$^{fx/+}$ (A) and *Nog*$^{fx/+}$;*Grem1*$^{fx/fx}$ (B) embryos display normal *Pax1* expression. (C) *Pax1* expression in *Nog*$^{fx/fx}$;*Grem1*$^{fx/+}$ embryos is normal in anterior somites but is lost posterior to the thoracic region. (D) A *Nog*$^{fx/fx}$;*Grem1*$^{fx/fx}$ double-mutant embryo lacking *Pax1* expression in the sclerotome but retaining expression in the pharyngeal arches (arrowheads). (**E-H**) Whole-mount E9.5 in situ hybridizations for *Pax3*; lateral views. (E,F) *Nog*$^{fx/+}$;*Grem1*$^{fx/+}$ (E) and *Nog*$^{fx/+}$;*Grem1*$^{fx/fx}$ (F) embryos display normal *Pax3* expression in dermomyotome and dorsal neural tube. (G,H) *Pax3* expression in *Nog*$^{fx/fx}$;*Grem1*$^{fx/+}$ (G) and *Nog*$^{fx/fx}$;*Grem1*$^{fx/fx}$ (H) embryos is reduced in anterior somites (H, arrows). Somitic *Pax3* expression does not appear posterior to somite 13 but is retained in the dorsal neural tube (bracket).

Nog;Grem1 double-mutant embryos lack sclerotome

BMP signaling has both inductive and repressive functions in axial skeleton development. To reveal what effect *Nog* and *Grem1* ablation has on sclerotome induction, we analyzed the early expression of sclerotome markers. Paired domain transcription factor family member *Pax1* is one of the earliest markers of sclerotome and is required for normal vertebral development (Wilm et al., 1998). As expected, *Nog*$^{fx/+}$;*Grem1*$^{fx/+}$ control and *Grem1* mutant (*Nog*$^{fx/+}$;*Grem1*$^{fx/fx}$) embryos exhibited normal *Pax1* expression from E8.5 to E9.5 (Fig. 3A,B). *Pax1* transcript was also detected in E9.5 *Nog* mutant (*Nog*$^{fx/fx}$;*Grem1*$^{fx/+}$) somites, although, as with *Meox1*, expression was not present posterior to somite 15 (Fig. 3C). However, embryos mutant for both *Nog* and *Grem1* exhibited a striking loss of somitic *Pax1* expression at all stages examined, from E8.5 to E9.5 (Fig. 3D). Most (11 of 18) had no detectable somitic *Pax1* expression, whereas others showed residual, small expression domains within the five anteriormost somites. *Pax1* expression in the pharyngeal arches was present in all genetic classes.

We also analyzed the expression of *Pax9*, *Nkx3.2*, *Uncx4.1* (*Uncx* – Mouse Genome Informatics) and *Tbx18* in *Nog*;*Grem1* double-mutant embryos. Compared with *Pax1*, we observed an even greater effect of *Nog* and *Grem1* mutation on *Pax9* activation, which normally exhibits similar expression to *Pax1*. In contrast to the control and to *Nog* mutant or *Grem1* mutant embryos (see Fig. S2A-C in the supplementary material), we never observed *Pax9* expression in the somites of double mutants (see Fig. S2D in the supplementary material; *n*=5). However, expression remained in the pharyngeal arches and tail of all classes. Somitic expression of *Nkx3.2*, which in later axial skeleton development requires BMP for induction of cartilage genes (Zeng et al., 2002), was also absent specifically in *Nog*$^{fx/fx}$;*Grem1*$^{fx/+}$ embryos (see Fig. S2E-H in the supplementary material; *n*=4). *Uncx4.1* is required for the formation of pedicles, transverse processes and proximal ribs, which are derivatives of the lateral sclerotome (Leitges et al.,

2000). In the first 12-15 somites at E9.5, we observed *Uncx4.1* expression in the posterior compartment of the sclerotome of *Nog*$^{fx/+}$;*Grem1*$^{fx/+}$, *Nog*$^{fx/+}$;*Grem1*$^{fx/fx}$ and *Nog*$^{fx/fx}$;*Grem1*$^{fx/+}$ embryos. No expression was detected in the lumbar trunk of *Nog*$^{fx/fx}$;*Grem1*$^{fx/+}$ embryos, but expression was detected at the level of the hindlimbs. By contrast, expression in *Nog*$^{fx/fx}$;*Grem1*$^{fx/fx}$ was either absent (2 of 5) or sharply reduced (see Fig. S2L in the supplementary material). In the trunk, *Tbx18* marks the anterior epithelial somite (Kraus et al., 2001) and *Tbx18* loss of function results in reduced pedicles and proximal ribs (Bussen et al., 2004). We observed somitic *Tbx18* expression in *Nog*$^{fx/+}$;*Grem1*$^{fx/+}$, *Nog*$^{fx/+}$;*Grem1*$^{fx/fx}$ and *Nog*$^{fx/fx}$;*Grem1*$^{fx/+}$ embryos (see Fig. S2M-O in the supplementary material). In *Nog*$^{fx/fx}$;*Grem1*$^{fx/fx}$ embryos (see Fig. S2P in the supplementary material) somitic expression was markedly reduced (n=3) or absent (n=1). As both *Tbx18* and *Uncx4.1* are expressed throughout the respective anterior and posterior somite halves before becoming confined to the sclerotome, expression of these genes in some double mutants is not inconsistent with sclerotome deficiency. Rather, this analysis suggests that somite anterior-posterior pattern formation occurs in *Nog*$^{fx/fx}$;*Grem1*$^{fx/fx}$ embryos.

We next sought to rule out the possibility that *Nog*$^{fx/fx}$;*Grem1*$^{fx/fx}$ mutants have a generalized defect in somite differentiation. Another paired domain family member, *Pax3*, is expressed in the dorsal neural tube and dermomyotome at E9.5. In contrast to sclerotome markers, *Pax3* was expressed in the somites of all genetic classes (Fig. 3E-H). Control and *Grem1* mutant embryos showed normal E9.5 *Pax3* expression. Both *Nog* mutant (*Nog*$^{fx/fx}$;*Grem1*$^{fx/+}$) and *Nog*$^{fx/fx}$;*Grem1*$^{fx/fx}$ double-mutant (n=8) embryos showed diminished and disordered *Pax3* expression in the dermomyotome, reflective of compromised somite formation. Nevertheless, all embryos in both classes showed *Pax3* expression. Furthermore, the determinant of proliferating myoblasts, *Myf5*, was also expressed in *Nog*;*Grem1* double-mutant embryos (n=5), indicating that the early skeletal muscle program is maintained in the absence of these antagonists (see Fig. S3 in the supplementary material). To test the capacity of the double-mutant embryos to form lateral dermomyotome, we examined expression *Lbx1*, which encodes a transcription factor that marks myoblasts fated to form the skeletal muscle of the limbs. Similar to the other dermomyotomal markers analyzed, *Lbx1* was expressed at E9.5 in all genetic classes (see Fig. S3 in the supplementary material; n=5).

Although the expression of these transcripts was altered relative to controls, their presence indicates that *Nog*$^{fx/fx}$;*Grem1*$^{fx/fx}$ double mutants can form dermomyotome. Based on our analysis of tissue-specific markers, we conclude that deletion of *Nog* and *Grem1* specifically prevents induction of the sclerotome lineage in the recently formed somite. This phenotype is distinct from the somitogenesis defect shared by *Nog* and *Nog*;*Grem1* double mutants and is a novel instance of BMP antagonists with non-overlapping expression domains serving a cooperative function in organogenesis.

Later effects of antagonist mutation on sclerotome derivatives

The expected outcome of the failure to form sclerotome is the absence of an axial skeleton. However, *Nog*;*Grem1* double mutants do not survive to chondrogenic stages. We therefore tested the chondrogenic potential of *Nog*$^{fx/fx}$;*Grem1*$^{fx/fx}$ somites in micromass culture. Whereas *Nog*$^{fx/+}$;*Grem1*$^{fx/+}$ cultures showed numerous chondrogenic nodules after 6 days, *Nog*$^{fx/fx}$;*Grem1*$^{fx/fx}$ tissue failed to form any cartilage (see Fig. S4 in the supplementary material). We reasoned that differences in axial skeletal development among the genotypes that do survive to fetal stages might substantiate these findings in vivo. To define the contribution of *Grem1* heterozygosity to the *Nog* mutant phenotype, we stained E13.5 embryos with Alcian Blue to reveal cartilage morphology (Fig. 4). *Nog*$^{fx/fx}$ specimens were compared with the skeletons of *Nog*$^{fx/fx}$;*Grem1*$^{fx/+}$ animals, as well as with those of *Nog*$^{fx/+}$;*Grem1*$^{fx/+}$ controls and *Nog*$^{fx/+}$;*Grem1*$^{fx/fx}$ mutants. As the severity of the *Nog* mutant phenotype varies between strains, we were careful to maintain equivalent genetic backgrounds (Tylzanowski et al., 2006) (see Materials and methods).

Relative to *Nog*$^{fx/+}$;*Grem1*$^{fx/+}$ and *Nog*$^{fx/+}$;*Grem1*$^{fx/fx}$ specimens, which exhibited apparently normal development of the axial skeleton (Fig. 4A,B), *Nog*$^{fx/fx}$ mutants exhibited thickened ribs and vertebrae to approximately the anterior-posterior level of the twelfth to fifteenth vertebra (Fig. 4C; n=5). However, within the lumbar region, *Nog* mutants displayed reduced or absent axial cartilage. Dysmorphic condensations were present at the level of the hindlimbs. These defects were dramatically enhanced in *Nog* mutants additionally heterozygous for *Grem1* (Fig. 4D; n=3). Within the cervical spine, both the developing pedicles and lamina were diminished. These structures were not detected within the thoracic spine, where only the proximal aspects of the anteriormost ribs were present. In addition, there were no condensations marking the primordia of the vertebral bodies at any position. We did detect weakly staining reiterated condensations of undetermined identity within the posterior axis at the level of the hindlimb, suggesting that the expression of sclerotome markers observed in the posterior of E9.5 *Nog*$^{fx/fx}$;*Grem1*$^{fx/+}$ embryos can translate to a minimum of cartilage development.

These results prompted us to evaluate the contribution of *Grem1* heterozygosity to the sclerotome defects we had observed in *Nog*$^{fx/fx}$;*Grem1*$^{fx/+}$ animals at embryonic stages. Indeed, *Meox1* expression in E9.5 *Nog*$^{fx/fx}$ embryos revealed larger somites that extend posteriorly through the presumptive lumbar region (Fig. 4E; n=5), when compared with *Nog*$^{fx/fx}$;*Grem1*$^{fx/+}$ examples (Fig. 2G). Similarly, E9.5 *Nog*$^{fx/fx}$ *Pax1* expression appeared in more posterior aspects of the body axis (Fig. 4F; n=5). Based on our expression analysis for *Meox1* and *Pax1*, our qualitative assessment is that wherever somites form in either *Nog*$^{fx/fx}$;*Grem1*$^{fx/+}$ or *Nog*$^{fx/fx}$ embryos, a proportionally sized domain of sclerotome is induced. It is only in the absence of both *Nog* and *Grem1* that sclerotome specification and axial skeleton formation fail.

Taken together, these results show that the inactivation of even a single *Grem1* allele has dramatic consequences for the *Nog* mutant skeletal phenotype, confirming that these antagonists interact during sclerotome development. Furthermore, we suggest that these results define the BMP antagonist-dependent stage in sclerotome development. It is known that, following induction, sclerotome cells become mesenchymal and migrate laterally, medially and dorsally and become the primordia of ribs, spinous processes and vertebral bodies, respectively. The genetic programs directing morphogenesis of these different axial skeletal features are distinct. For example, *Uncx4.1* is specifically required for lateral sclerotome-derived ribs (Leitges et al., 2000), whereas *Pax1* and *Pax9* cooperate in the formation of the vertebral column (Peters et al., 1999). The generalized axial skeleton agenesis observed in *Nog*$^{fx/fx}$;*Grem1*$^{fx/+}$ animals suggests that *Nog* and *Grem1* function early in sclerotome development prior to the subdivision of the different sclerotome compartments.

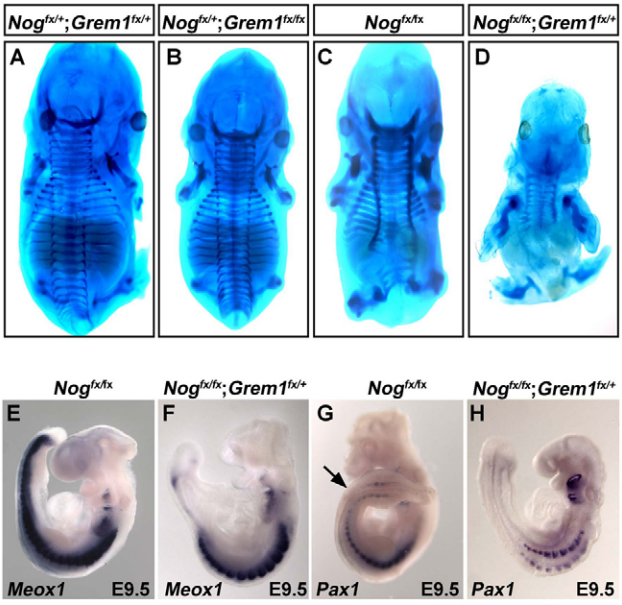

Fig. 4. Grem1 heterozygosity enhances the *Nog* mutant skeletal phenotype. (**A-D**) Whole-mount E13.5 mouse embryos stained with Alcian Blue to detect cartilage; dorsal views. (A,B) *Nog*$^{fx/+}$;*Grem1*$^{fx/+}$ (A) and *Nog*$^{fx/+}$;*Grem1*$^{fx/fx}$ (B) examples have normal axial skeletal morphology. (C) A *Nog*$^{fx/fx}$ mutant displaying thickened cervical and thoracic skeletal elements and reduced lumbar cartilage. (D) In *Nog*$^{fx/fx}$;*Grem1*$^{fx/+}$ animals, formation of the cartilage of the axial skeleton is dramatically impaired. (**E-H**) Whole-mount E9.5 in situ hybridizations for *Meox1* (E,F) and *Pax1* (G,H). (E,F) Although reduced relative to controls, this *Nog*$^{fx/fx}$ embryo (E) exhibits greater *Meox1* expression than a *Nog*$^{fx/fx}$;*Grem1*$^{fx/+}$ embryo (F). (G,H) *Pax1* expression in this *Nog*$^{fx/fx}$ embryo (G) appears in the lumbar region (arrow) to the level of the hindlimb buds, a region that does not express *Pax1* in the *Nog*$^{fx/fx}$;*Grem1*$^{fx/+}$ embryo (H).

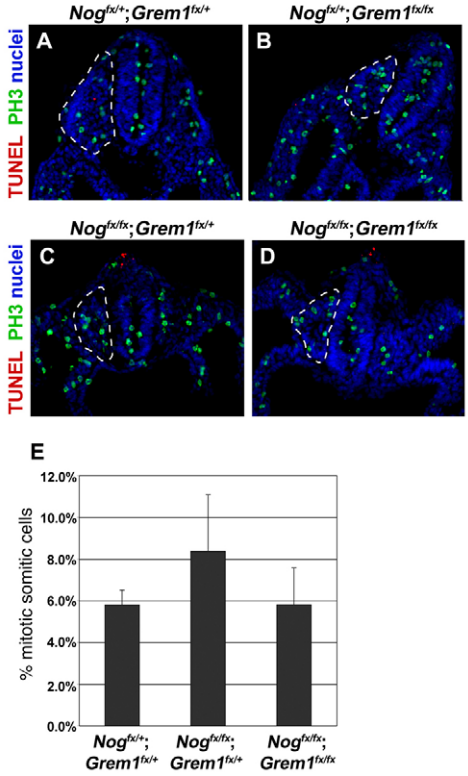

Fig. 5. Neither aberrant cell death nor proliferation explains sclerotome agenesis. (**A-D**) Transverse sections between somites 8-12 of E9.0 mouse embryos. TUNEL-positive cells (red) indicate cell death, whereas phosphorylated histone H3 (PH3)-positive cells (green) reveal mitosis, and Hoechst (blue) labels nuclei. (A,B) *Nog*$^{fx/+}$;*Grem1*$^{fx/+}$ control (A) and *Nog*$^{fx/+}$;*Grem1*$^{fx/fx}$ *Grem1* mutant (B) examples exhibit few apoptotic cells. (C,D) *Nog*$^{fx/fx}$;*Grem1*$^{fx/+}$ *Nog* mutant (C) and *Nog*$^{fx/fx}$;*Grem1*$^{fx/fx}$ double-mutant (D) examples exhibit apoptotic cells in the dorsal neural tube (arrows). No overt differences in somitic PH3-positive cells were observed among the different genotypes. Dashed lines indicate somite perimeters. (**E**) Bar chart showing mitotic cells within the somite as a percentage of all somitic nuclei. The three genetic classes analyzed – control *Nog*$^{fx/+}$;*Grem1*$^{fx/+}$ (left), *Nog* mutant *Nog*$^{fx/fx}$;*Grem1*$^{fx/-}$ (center), and double-mutant *Nog*$^{fx/fx}$;*Grem1*$^{fx/fx}$ (right) – exhibited no significant differences in somitic proliferation rates. A minimum of three embryos of each genotype were analyzed, and at least five sections from each embryo were counted. Error bars indicate 2× s.e.m.

Aberrant cell death and proliferation do not explain sclerotome agenesis

We next sought to ascertain the basis of the failure to form sclerotome in *Nog*$^{fx/fx}$;*Grem1*$^{fx/fx}$ double mutants. Either cell death, or a failure to proliferate, or a combination of these two forces early in the sclerotome lineage could explain the absence of axial skeleton progenitors. As the *Nog*$^{fx/fx}$;*Grem1*$^{fx/fx}$ mutant phenotype is detectable by E9.0, any aberrant cell death or proliferation would have to occur prior to this stage. We dissected trunk tissue spanning somites 8-12 from embryos in the process of turning (Theiler stages 13-14). These somites are recently formed (based on 120-minute periodicity, they are between 2 and 8 hours old) and, in double mutants, represent a position at which somites exist but sclerotome markers are never observed. Sections processed for TUNEL staining from *Nog*$^{fx/+}$;*Grem1*$^{fx/+}$ control and *Nog*$^{fx/+}$;*Grem1*$^{fx/fx}$ mutant samples did not reveal any pattern of cell death (Fig. 5A,B). The dorsal neural tube of E10.5 *Nog* mutant embryos exhibits high levels of apoptosis (McMahon et al., 1998) (Fig. 5C). We detected similar TUNEL-positive cells in the dorsal neural tube of *Nog*$^{fx/fx}$;*Grem1*$^{fx/+}$ and *Nog*$^{fx/fx}$;*Grem1*$^{fx/fx}$ embryos at E9.0 (Fig. 5D). However, very few apoptotic cells were detected in other structures.

Although the thoracic-level somites of E8.5-9.0 *Nog*$^{fx/fx}$;*Grem1*$^{fx/fx}$ double mutants were smaller than those of controls, there was no apparent size difference between double mutants and *Nog* mutants. Nevertheless, cell cycle defects within the ventral-medial somite could contribute to the sclerotome-deficient phenotype. We stained sections for phosphorylated histone H3 (PH3) to determine the rates of proliferation in control, *Nog* and *Nog*;*Grem1* double mutants. Based on morphology, we estimated the perimeter of the somite within a transverse section. To calculate proliferation rate, we expressed the number of PH3-positive cells as a percentage of the total number of nuclei within the defined somite area (Fig. 5E). We did not find any significant difference between proliferation in the paraxial mesoderm of *Nog*$^{fx/+}$;*Grem1*$^{fx/+}$, *Nog*$^{fx/fx}$;*Grem1*$^{fx/+}$ or *Nog*$^{fx/fx}$;*Grem1*$^{fx/fx}$ embryos: in all three classes, 6-8% of cells were dividing.

These data suggest that at the stages at which *Nog* and *Grem1* are likely to function in sclerotome patterning, there are no differences in either the rates of somitic mitosis or cell death for the different genetic classes. Although we cannot exclude the

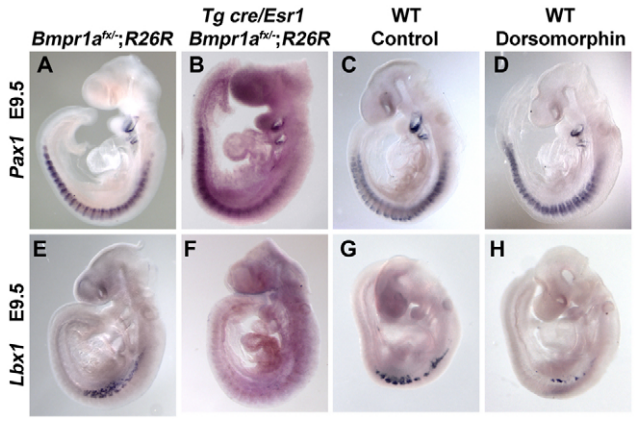

Fig. 6. Inhibition of BMP signaling does not enhance sclerotome formation. Whole-mount E9.5 in situ hybridizations for mouse *Pax1*(A-D) and *Lbx1* (E-H); lateral views. (**A**,**B**,**E**,**F**) Conditional *Bmpr1a* mutants. Tamoxifen was administered via the mother at E7.5, 40 hours before dissection. Embryos were processed for β-galactosidase activity (pink) prior to in situ hybridization. *Bmpr1a*$^{fx/-}$;*R26R* controls displaying normal *Pax1* (A, *n*=6) and *Lbx1* (E, *n*=4) expression. *Bmpr1a*$^{fx/-}$;*R26R*;*Tg*(*Cre/Esr1*) embryos express *Pax1* (B, *n*=5) normally but do not express *Lbx1* (F, *n*=4). (**C**,**D**,**G**,**H**) Embryos cultured from E8.5 for 30 hours in DMSO vehicle alone (C,G) or 2.5 μM dorsomorphin (D,H). Dorsomorphin does not interfere with *Pax1* expression (D) but does block *Lbx1* induction (H). At least five embryos of each condition were analyzed. WT, wild type.

possibility that our analysis missed a critical stage, our data indicate that the failure to form sclerotome is not a consequence of early cell death or a lack of proliferation. Rather, we hypothesize that cells within the ventral somite of *Nog*;*Grem1* mutant embryos fail to receive or interpret the signals necessary for sclerotome specification.

Inhibition of BMP signaling in a *Nog*$^{+/+}$ *Grem1*$^{+/+}$ background does not influence sclerotome formation

As a complement to our analysis of mutants lacking BMP antagonist gene function, we also examined sclerotome induction following interference with BMP signaling. We employed two strategies to block BMP signal transduction. First, we used conditional mutants for the type I BMP receptor *Bmpr1a* (Fig. 6A,B,E,F). We generated males heterozygous for a *Bmpr1a* null allele (Mishina et al., 1995) that also bear the ubiquitously expressed tamoxifen-inducible estrogen receptor fused to Cre recombinase [*Bmpr1a*$^{+/-}$;*Tg*(*Cre/Esr1*)] (Hayashi et al., 2002). These animals were crossed to females homozygous for both the *Bmpr1a* conditional allele and the Rosa26 reporter (*Bmpr1a*$^{fx/fx}$;*R26R*) (Mishina et al., 2002; Soriano, 1999). Tamoxifen was administered at E7.5 and animals were analyzed at E9.5. Embryos with the genotype *Bmpr1a*$^{fx/-}$;*Tg*(*Cre/Esr1*) stained strongly for β-galactosidase, suggesting high levels of Cre recombinase activity (Fig. 6B,F). However, these embryos showed no change in *Pax1* expression when compared with siblings that did not express Cre (Fig. 6B; see Fig. S5 in the supplementary material). By contrast, *Lbx1* expression was absent or dramatically reduced in these *Bmpr1a* conditional mutants (Fig. 6F; see Fig. S5 in the supplementary material). As BMP signals are involved in the induction of lateral dermomyotome derivatives (Hirsinger et al., 1997; Pourquie et al., 1996; Tonegawa et al., 1997), this observation demonstrates the efficacy of this conditional mutagenesis approach. Nevertheless, we saw no change in sclerotome development resulting from *Bmpr1a* conditional mutation.

To corroborate these findings, we used the drug dorsomorphin to block type I BMP receptor function in cultured whole embryos (Yu et al., 2008). Embryos were cultured from E8.5 for 30 hours in media supplemented with either 2.5 μM dorsomorphin (Fig. 6D,H) or DMSO vehicle alone (Fig. 6C,G). Control embryos generally appeared morphologically normal and expressed normal levels of *Pax1* and *Lbx1*. Exposure to dorsomorphin did not interfere with somitogenesis, turning or neural tube closure but did result in blistering of the epidermis, associated hematomas and underdevelopment of the allantois. As in *Bmpr1a* conditional mutants, *Pax1* was expressed normally, whereas *Lbx1* expression was either diminished or lost.

These data show that the inhibition of BMP signal transduction beyond the levels normally mediated by Nog and Grem1 does not result in a bias toward sclerotome in the newly formed somite. Our findings are consistent with a model in which the function of BMP antagonists in the developing trunk is to block a BMP signal that suppresses sclerotome induction, rather than to provide an instructive signal.

Elevated BMP signaling prevents Hh-dependent sclerotome specification

The absence of BMP antagonists should result in elevated BMP signaling. To prove that the failure to form sclerotome in *Nog*$^{fx/fx}$;*Grem1*$^{fx/fx}$ embryos is a consequence of excessive BMP signaling, we cultured double-mutant embryos from E8.5 for 30 hours in media supplemented with either 2.5 μM dorsomorphin or DMSO vehicle alone. In all cases (16/16), *Pax1* expression was rescued in dorsomorphin-treated double-mutant specimens (Fig. 7A,B).

We next sought to define how elevated BMP signaling interferes with sclerotome induction. Hh signaling is required for sclerotome development (Zhang et al., 2001). However, in a previous study using explanted paraxial mesoderm, sclerotome marker expression was triggered in response to Nog even after pharmacological inhibition of Hh signaling, suggesting the possibility of an Hh-independent sclerotome induction mechanism (McMahon et al., 1998). However, we found that inhibition of BMP signaling with 2.5 μM dorsomorphin failed to rescue *Pax1* expression in *Smo* null embryos (*n*=2), demonstrating that even in a BMP signaling-deficient state, Hh signaling is essential for sclerotome specification (Fig. 7B,C).

We reasoned that compromised Hh signaling within the developing somites could explain the absence of sclerotome in *Nog*$^{fx/fx}$;*Grem1*$^{fx/fx}$ embryos. To characterize the state of Hh signaling, we compared control and mutant E9.0 expression of *Shh*, the Hh signaling-inhibitory receptor *Ptc* (*Ptch1* – Mouse Genome Informatics) and the Gli transcription factors that mediate the transcription of Hh-regulated genes (Fig. 7E-G). *Shh* transcript was detected in all genetic classes, suggesting that Shh is produced in *Nog*$^{fx/fx}$;*Grem1*$^{fx/fx}$ double mutants (not shown). We reasoned that *Ptc* and *Gli1*, which are directly regulated by Hh signaling (Buttitta et al., 2003; Dockter and Ordahl, 2000), would best indicate functional Hh signaling. We were surprised to observe *Ptc* expression in the compartment that normally becomes sclerotome (Fig. 7G, inset). Moreover, somitic expression of *Gli1*, *Gli2* and *Gli3* (Fig. 7H-M; data not shown)

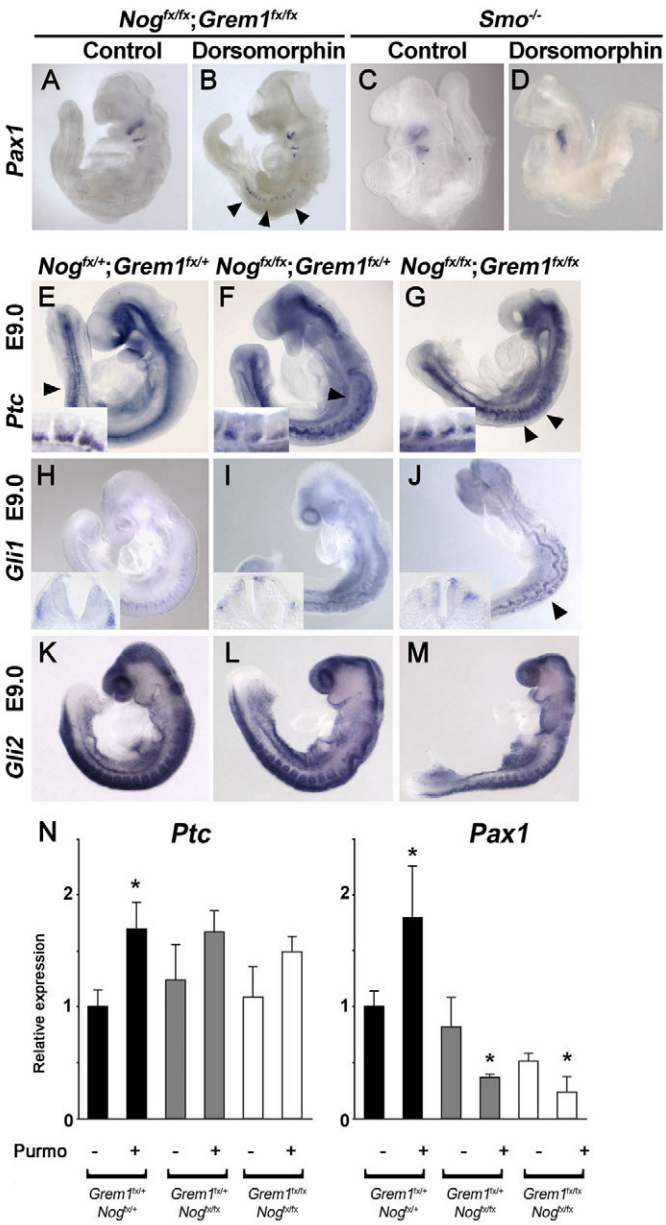

Fig. 7. Elevated BMP signaling in mouse *Nog;Grem1* double mutants interferes with Hh signaling. (**A-M**) Whole-mount in situ hybridizations for *Pax1* (A-D), *Ptc* (E-G), *Gli1* (H-J) and *Gli2* (K-M); lateral views, facing left. (A-D) $Nog^{fx/fx}$;$Grem1^{fx/fx}$ (A,B) and $Smo^{-/-}$ (C,D) embryos, cultured from E8.5 for 30 hours in DMSO vehicle alone (A,C) or 2.5 μM dorsomorphin (B,D). Dorsomorphin restores somitic *Pax1* expression as well as some posterior somite formation in $Nog^{fx/fx}$;$Grem1^{fx/fx}$ embryos (B) (arrowheads) but does not rescue *Pax1* expression in the absence of Hh signaling (D). (E-M) $Nog^{fx/+}$;$Grem1^{fx/+}$ (E,H,K), $Nog^{fx/fx}$;$Grem1^{fx/+}$ (F,I,L) and $Nog^{fx/fx}$;$Grem1^{fx/fx}$ (G,J,M) embryos. *Ptc*, *Gli1* and *Gli2* are expressed in all genetic classes. (E-G) Note reiterated *Ptc* expression in somites (arrowheads). Insets are midline lateral views of similarly staged embryos bisected at the level of the forelimb, revealing ventral medial *Ptc* expression. (J) Although reduced, *Gli1* was detected in $Nog^{fx/fx}$;$Grem1^{fx/fx}$ embryos (arrowhead). Insets are transverse sections through somite 10, revealing somite expression. (**N**) QPCR analysis of *Ptc* and *Pax1* expression for control (black bars), *Nog* mutant (gray bars) or *Nog*;*Grem1* double-mutant (white bars) embryos cultured with purmorphamine or vehicle alone. *Ptc* expression increases in response to smoothened activation in all genotypes. *Pax1* expression is elevated in response to purmorphamine in controls but decreased in antagonist mutants. A minimum of three embryos were used for each condition. Expression for mock-treated $Nog^{fx/+}$;$Grem1^{fx/+}$ controls was set to 1. Error bars indicate 2× s.e.m. *, $P<0.05$ between purmorphamine- and control-treated embryos of that genotype.

was detected in $Nog^{fx/fx}$;$Grem1^{fx/fx}$ embryos. We conclude that key genes that mediate Hh signal transduction are expressed and induced at relatively normal levels in the somites of double mutants.

To further test the hypothesis that sclerotome deficiency might be a consequence of defective Hh signal transduction, we again used whole-embryo culture. We treated E8.5 embryos for 30 hours in media supplemented with either 7.5 μM purmorphamine or vehicle alone. Purmorphamine activates the Hh pathway by targeting Smo (Sinha and Chen, 2006). This manipulation induced a significant increase in the expression of *Ptc* and *Pax1* in $Nog^{fx/+}$;$Grem1^{fx/+}$ control embryos, as indicated by QPCR (Fig. 7N). Likewise, *Ptc* expression was elevated following purmorphamine treatment in both $Nog^{fx/fx}$;$Grem1^{fx/+}$ and $Nog^{fx/fx}$;$Grem1^{fx/fx}$ samples. However, we were surprised to find *Pax1* expression significantly reduced following Smo activation. In addition, we never detected somitic *Pax1* expression by in situ hybridization in purmorphamine-treated $Nog^{fx/fx}$;$Grem1^{fx/fx}$ embryos (n=3; data not shown). The failure to respond to Smo activation strongly suggests that Hh signaling leading to *Pax1* activation is defective in BMP antagonist mutants. We propose that a BMP-mediated alteration in the response to Hh signaling in the somite is the basis of sclerotome agenesis in $Nog^{fx/fx}$;$Grem1^{fx/fx}$ double mutants. Furthermore, these data show that BMP signaling can produce a specific switch in how the Hh signal is interpreted.

DISCUSSION

Our analysis shows that Nog and Grem1 cooperate to maintain a zone of reduced BMP signaling within the naïve somite that is essential for sclerotome specification. Ablation of *Nog* and *Grem1* results in elevated BMP signaling that interferes with Hh signal transduction crucial for sclerotome induction at a step downstream of Smo. This work expands our understanding of the genetics underlying sclerotome induction, defining a developmental mechanism in which two factors secreted from different source tissues act together in pattern formation. Furthermore, our findings reveal an important example of how BMP signaling can restrict the consequences of Hh signal transduction.

BMP blocks specification of axial skeleton progenitors

Our findings confirm that BMP signaling must be attenuated during the specification of the cells that go on to form the axial skeleton. Once the ventral medial somite has committed to the sclerotome lineage, BMP has a positive role in the growth and elaboration of the axial skeleton (Monsoro-Burq et al., 1996; Murtaugh et al., 1999) by maintaining an Nkx3.2- and Sox9-dependent chondrogenic regulatory loop (Zeng et al., 2002). The expression of *Nog* in the notochord and *Grem1* in the somite reflects this transition: coincident with sclerotome specification, which occurs at ~E9.0 for the thoracic region, antagonist expression in these domains begins to diminish.

Our findings are consistent with a model of sclerotome induction in which Hh is the only instructive signal required. It has been hypothesized that Nog might also direct sclerotome specification (McMahon et al., 1998). Although the work presented here does not prove that Nog cannot mediate Hh-independent sclerotome induction, we have no evidence supporting such a mechanism in vivo. Rather, our data suggest that BMP antagonists act to provide a permissive environment for sclerotome specification. Neither genetic nor pharmacological interference with BMP signaling results in a bias toward the sclerotome fate, as would be predicted if BMP antagonists were driving differentiation. Furthermore, in an embryo incapable of Hh signal transduction owing to *Smo* ablation, blocking BMP signaling does not restore sclerotome marker expression.

In addition to the sclerotome, the loss of *Nog* and *Grem1* has consequences for other axial tissues. Development of the dermomyotome is also perturbed in *Nog* and *Nog*;*Grem1* double mutants, as indicated by diminished *Pax3* and *Myf5* expression. A possible explanation for reduced expression lies in the overall smaller size of somites in these embryos. However, BMP-mediated interference with the development of dermomyotome could be consistent with our results and our understanding of early myogenesis. Hh signaling is required for efficient dermomyotome induction (Borello et al., 2006; Borycki et al., 1999; Chiang et al., 1996; Gustafsson et al., 2002; Teboul et al., 2003; Zhang et al., 2001). The defective Hh signaling that results from elevated BMP signaling may also cause defective dermomyotome development. Finally, it should be noted that although our analysis focuses on the role of BMP antagonists in somite pattern formation, we also found that excessive BMP signaling interferes with somite formation. This observation is consistent with the ability of BMP antagonists to induce somitic fates in *Xenopus* explants that are specified as ventral mesoderm, and to induce ectopic somites in chick lateral plate (Smith et al., 1993; Tonegawa et al., 1997). How BMP interferes with the somite formation process is not known.

BMP interferes with Hh target transactivation

Defining how signaling pathways interact is crucial for understanding cell fate decisions. Our analysis shows that, within the somite, BMP signaling results in selected disruption of Hh signaling, as indicated by the failure of Smo activation to induce expression of the sclerotome marker *Pax1* in $Nog^{fx/fx}$;$Grem1^{fx/fx}$ embryos. As we have detected transcripts of components of the Hh signaling machinery, including the transcription factors *Gli2* and *Gli3* that are required for sclerotome (Buttitta et al., 2003), we hypothesize that elevated BMP signaling results in the production of a dominant repressor of *Pax1* expression in *Nog*;*Grem1* double mutants. We argue that this effect is selective, as Hh signal transduction and activation of gene expression are still effective in activating *Ptc*. The surprising reduction in *Pax1* expression elicited by purmorphamine in $Nog^{fx/fx}$;$Grem1^{fx/+}$ and $Nog^{fx/fx}$;$Grem1^{fx/fx}$ embryos suggests that the context of BMP activation converts the activating Hh signal to a repressive one. Alternatively, BMP leads to a dominant repressive activity on the *Pax1* promoter.

A mechanism in which BMP signaling functions in opposition to Shh signaling is not without precedent. In the ventral neural tube, which is patterned by notochord- and floor plate-derived Shh, BMPs induce more dorsal cell types, although in this context the dose of BMP is instructive (Liem et al., 2000; Timmer et al., 2002). Conversely, zebrafish bearing mutations in BMP pathway components exhibit a ventralized neural tube (Barth et al., 1999). In cerebellar granule neuron progenitors and primary medulloblastoma cells, Shh-dependent proliferation is blocked by BMP-induced degradation of the Hh target *Atoh1* (*Math1*) (Zhao et al., 2008). It will be important to define the differences between the transactivation of contextual targets of Hh signaling, such as *Pax1* in the sclerotome, and invariant targets, such as *Ptc*, in different Hh-responsive cell types as well as how other developmental pathways affect the transcriptional readout. As a general word of caution, this work also demonstrates that active Ptc expression does not necessarily imply that the Hh signal transduction leading to other Hh targets is functioning normally.

Nog and Grem1 cooperate despite derivation from different sources

Nog and *Grem1* are not the only BMP antagonists expressed in the embryonic trunk. *Chrd* is expressed in the node and later in the notochord and follistatin is expressed in the PSM and the developing somites. It might be significant that approximately one-third of *Nog*;*Grem1* double mutants exhibit faint expression of *Pax1* in anterior somites. This limited sclerotome induction could be a result of compensation from additional BMP antagonists. Notably, the expression domains of *Nog* and *Grem1* do not overlap. We suggest that the cooperative function of signals secreted from different source tissues might be a common feature of developing systems. With regard to the developing skeleton and the signaling pathways involved, a wide array of genes with different expression domains but overlapping functions might have been a significant factor in generating diversity in skeletal forms.

Acknowledgements

We thank Yuji Mishina for generously providing the *Bmpr1a* conditional and null lines; Jeremy Reiter for *Smo* mutant animals; Debbie Pangilinan for animal care; and Mike Sohaskey for critical comments on the manuscript. This work is supported by the American Cancer Society Postdoctoral Fellowship in memory of Dorothy Forbes and NIH GM49346. Deposited in PMC for release after 12 months.

Competing interests statement

The authors declare no competing financial interests.

Supplementary material

Supplementary material for this article is available at
http://dev.biologists.org/lookup/suppl/doi:10.1242/dev.051938/-/DC1

References

Bachiller, D., Klingensmith, J., Kemp, C., Belo, J. A., Anderson, R. M., May, S. R., McMahon, J. A., McMahon, A. P., Harland, R. M., Rossant, J. et al. (2000). The organizer factors Chordin and Noggin are required for mouse forebrain development. *Nature* **403**, 658-661.

Barth, K. A., Kishimoto, Y., Rohr, K. B., Seydler, C., Schulte-Merker, S. and Wilson, S. W. (1999). Bmp activity establishes a gradient of positional information throughout the entire neural plate. *Development* **126**, 4977-4987.

Borello, U., Berarducci, B., Murphy, P., Bajard, L., Buffa, V., Piccolo, S., Buckingham, M. and Cossu, G. (2006). The Wnt/beta-catenin pathway regulates Gli-mediated Myf5 expression during somitogenesis. *Development* **133**, 3723-3732.

Borycki, A. G., Mendham, L. and Emerson, C. P., Jr (1998). Control of somite patterning by Sonic hedgehog and its downstream signal response genes. *Development* **125**, 777-790.

Borycki, A. G., Brunk, B., Tajbakhsh, S., Buckingham, M., Chiang, C. and Emerson, C. P., Jr (1999). Sonic hedgehog controls epaxial muscle determination through Myf5 activation. *Development* **126**, 4053-4063.

Brunet, L. J., McMahon, J. A., McMahon, A. P. and Harland, R. M. (1998). Noggin, cartilage morphogenesis, and joint formation in the mammalian skeleton. *Science* **280**, 1455-1457.

Bussen, M., Petry, M., Schuster-Gossler, K., Leitges, M., Gossler, A. and Kispert, A. (2004). The T-box transcription factor Tbx18 maintains the separation of anterior and posterior somite compartments. *Genes Dev.* **18**, 1209-1221.

Buttitta, L., Mo, R., Hui, C. C. and Fan, C. M. (2003). Interplays of Gli2 and Gli3 and their requirement in mediating Shh-dependent sclerotome induction. *Development* **130**, 6233-6243.

Candia, A. F., Hu, J., Crosby, J., Lalley, P. A., Noden, D., Nadeau, J. H. and Wright, C. V. (1992). Mox-1 and Mox-2 define a novel homeobox gene subfamily and are differentially expressed during early mesodermal patterning in mouse embryos. *Development* **116**, 1123-1136.
Chiang, C., Litingtung, Y., Lee, E., Young, K. E., Corden, J. L., Westphal, H. and Beachy, P. A. (1996). Cyclopia and defective axial patterning in mice lacking Sonic hedgehog gene function. *Nature* **383**, 407-413.
Dockter, J. and Ordahl, C. P. (2000). Dorsoventral axis determination in the somite: a re-examination. *Development* **127**, 2201-2206.
Fan, C. M. and Tessier-Lavigne, M. (1994). Patterning of mammalian somites by surface ectoderm and notochord: evidence for sclerotome induction by a hedgehog homolog. *Cell* **79**, 1175-1186.
Gazzerro, E., Smerdel-Ramoya, A., Zanotti, S., Stadmeyer, L., Durant, D., Economides, A. N. and Canalis, E. (2007). Conditional deletion of gremlin causes a transient increase in bone formation and bone mass. *J. Biol. Chem.* **282**, 31549-31557.
Gustafsson, M. K., Pan, H., Pinney, D. F., Liu, Y., Lewandowski, A., Epstein, D. J. and Emerson, C. P., Jr (2002). Myf5 is a direct target of long-range Shh signaling and Gli regulation for muscle specification. *Genes Dev.* **16**, 114-126.
Hayashi, S., Lewis, P., Pevny, L. and McMahon, A. P. (2002). Efficient gene modulation in mouse epiblast using a Sox2Cre transgenic mouse strain. *Mech. Dev.* **119**, S97-S101.
Hirsinger, E., Duprez, D., Jouve, C., Malapert, P., Cooke, J. and Pourquie, O. (1997). Noggin acts downstream of Wnt and Sonic Hedgehog to antagonize BMP4 in avian somite patterning. *Development* **124**, 4605-4614.
Hsu, D. R., Economides, A. N., Wang, X., Eimon, P. M. and Harland, R. M. (1998). The Xenopus dorsalizing factor Gremlin identifies a novel family of secreted proteins that antagonize BMP activities. *Mol. Cell* **1**, 673-683.
Khokha, M. K., Hsu, D., Brunet, L. J., Dionne, M. S. and Harland, R. M. (2003). Gremlin is the BMP antagonist required for maintenance of Shh and Fgf signals during limb patterning. *Nat. Genet.* **34**, 303-307.
Kraus, F., Haenig, B. and Kispert, A. (2001). Cloning and expression analysis of the mouse T-box gene Tbx18. *Mech. Dev.* **100**, 83-86.
Leitges, M., Neidhardt, L., Haenig, B., Herrmann, B. G. and Kispert, A. (2000). The paired homeobox gene Uncx4.1 specifies pedicles, transverse processes and proximal ribs of the vertebral column. *Development* **127**, 2259-2267.
Lewandoski, M., Meyers, E. N. and Martin, G. R. (1997). Analysis of Fgf8 gene function in vertebrate development. *Cold Spring Harb. Symp. Quant. Biol.* **62**, 159-168.
Liem, K. F., Jr, Jessell, T. M. and Briscoe, J. (2000). Regulation of the neural patterning activity of sonic hedgehog by secreted BMP inhibitors expressed by notochord and somites. *Development* **127**, 4855-4866.
Mankoo, B. S., Skuntz, S., Harrigan, I., Grigorieva, E., Candia, A., Wright, C. V., Arnheiter, H. and Pachnis, V. (2003). The concerted action of Meox homeobox genes is required upstream of genetic pathways essential for the formation, patterning and differentiation of somites. *Development* **130**, 4655-4664.
Marcelle, C., Ahlgren, S. and Bronner-Fraser, M. (1999). In vivo regulation of somite differentiation and proliferation by Sonic Hedgehog. *Dev. Biol.* **214**, 277-287.
McMahon, J. A., Takada, S., Zimmerman, L. B., Fan, C. M., Harland, R. M. and McMahon, A. P. (1998). Noggin-mediated antagonism of BMP signaling is required for growth and patterning of the neural tube and somite. *Genes Dev.* **12**, 1438-1452.
Mishina, Y., Suzuki, A., Ueno, N. and Behringer, R. R. (1995). Bmpr encodes a type I bone morphogenetic protein receptor that is essential for gastrulation during mouse embryogenesis. *Genes Dev.* **9**, 3027-3037.
Mishina, Y., Hanks, M. C., Miura, S., Tallquist, M. D. and Behringer, R. R. (2002). Generation of Bmpr/Alk3 conditional knockout mice. *Genesis* **32**, 69-72.
Monsoro-Burq, A. H., Duprez, D., Watanabe, Y., Bontoux, M., Vincent, C., Brickell, P. and Le Douarin, N. (1996). The role of bone morphogenetic proteins in vertebral development. *Development* **122**, 3607-3616.
Murtaugh, L. C., Chyung, J. H. and Lassar, A. B. (1999). Sonic hedgehog promotes somitic chondrogenesis by altering the cellular response to BMP signaling. *Genes Dev.* **13**, 225-237.
Nagy, A., Gersenstein, M., Vintersten, K. and Behringer, R. (2003). *Manipulating the Mouse Embryo: a Laboratory Manual* (3rd edn). Cold Spring Harbor, NY: Cold Spring Harbor Laboratory Press.
Pearce, J. J., Penny, G. and Rossant, J. (1999). A mouse cerberus/Dan-related gene family. *Dev. Biol.* **209**, 98-110.
Peters, H., Wilm, B., Sakai, N., Imai, K., Maas, R. and Balling, R. (1999). Pax1 and Pax9 synergistically regulate vertebral column development. *Development* **126**, 5399-5408.
Pourquie, O., Fan, C. M., Coltey, M., Hirsinger, E., Watanabe, Y., Breant, C., Francis-West, P., Brickell, P., Tessier-Lavigne, M. and Le Douarin, N. M. (1996). Lateral and axial signals involved in avian somite patterning: a role for BMP4. *Cell* **84**, 461-471.
Sinha, S. and Chen, J. K. (2006). Purmorphamine activates the Hedgehog pathway by targeting Smoothened. *Nat. Chem. Biol.* **2**, 29-30.
Smith, W. C., Knecht, A. K., Wu, M. and Harland, R. M. (1993). Secreted noggin protein mimics the Spemann organizer in dorsalizing Xenopus mesoderm. *Nature* **361**, 547-549.
Soriano, P. (1999). Generalized lacZ expression with the ROSA26 Cre reporter strain. *Nat. Genet.* **21**, 70-71.
Teboul, L., Summerbell, D. and Rigby, P. W. (2003). The initial somitic phase of Myf5 expression requires neither Shh signaling nor Gli regulation. *Genes Dev.* **17**, 2870-2874.
Teillet, M., Watanabe, Y., Jeffs, P., Duprez, D., Lapointe, F. and Le Douarin, N. M. (1998). Sonic hedgehog is required for survival of both myogenic and chondrogenic somitic lineages. *Development* **125**, 2019-2030.
Timmer, J. R., Wang, C. and Niswander, L. (2002). BMP signaling patterns the dorsal and intermediate neural tube via regulation of homeobox and helix-loop-helix transcription factors. *Development* **129**, 2459-2472.
Tonegawa, A., Funayama, N., Ueno, N. and Takahashi, Y. (1997). Mesodermal subdivision along the mediolateral axis in chicken controlled by different concentrations of BMP-4. *Development* **124**, 1975-1984.
Tylzanowski, P., Mebis, L. and Luyten, F. P. (2006). The Noggin null mouse phenotype is strain dependent and haploinsufficiency leads to skeletal defects. *Dev. Dyn.* **235**, 1599-1607.
Wijgerde, M., Karp, S., McMahon, J. and McMahon, A. P. (2005). Noggin antagonism of BMP4 signaling controls development of the axial skeleton in the mouse. *Dev. Biol.* **286**, 149-157.
Wilm, B., Dahl, E., Peters, H., Balling, R. and Imai, K. (1998). Targeted disruption of Pax1 defines its null phenotype and proves haploinsufficiency. *Proc. Natl. Acad. Sci. USA* **95**, 8692-8697.
Winnier, G. E., Hargett, L. and Hogan, B. L. (1997). The winged helix transcription factor MFH1 is required for proliferation and patterning of paraxial mesoderm in the mouse embryo. *Genes Dev.* **11**, 926-940.
Yu, P. B., Hong, C. C., Sachidanandan, C., Babitt, J. L., Deng, D. Y., Hoyng, S. A., Lin, H. Y., Bloch, K. D. and Peterson, R. T. (2008). Dorsomorphin inhibits BMP signals required for embryogenesis and iron metabolism. *Nat. Chem. Biol.* **4**, 33-41.
Zeng, L., Kempf, H., Murtaugh, L. C., Sato, M. E. and Lassar, A. B. (2002). Shh establishes an Nkx3.2/Sox9 autoregulatory loop that is maintained by BMP signals to induce somitic chondrogenesis. *Genes Dev.* **16**, 1990-2005.
Zhang, X. M., Ramalho-Santos, M. and McMahon, A. P. (2001). Smoothened mutants reveal redundant roles for Shh and Ihh signaling including regulation of L/R symmetry by the mouse node. *Cell* **106**, 781-792.
Zhao, H., Ayrault, O., Zindy, F., Kim, J. H. and Roussel, M. F. (2008). Post-transcriptional down-regulation of Atoh1/Math1 by bone morphogenic proteins suppresses medulloblastoma development. *Genes Dev.* **22**, 722-727.
Zimmerman, L. B., De Jesus-Escobar, J. M. and Harland, R. M. (1996). The Spemann organizer signal noggin binds and inactivates bone morphogenetic protein 4. *Cell* **86**, 599-606.